

Alignment effects in odd-mass Cs isotopes: Spectroscopy of ^{125}Cs

J. R. Hughes, D. B. Fossan, D. R. LaFosse, Y. Liang, P. Vaska, and M. P. Waring

Department of Physics, State University of New York at Stony Brook, Stony Brook, New York 11794

(Received 15 August 1991)

Several rotational bands have been populated in the $Z = 55$ nucleus ^{125}Cs using the fusion evaporation reaction $^{110}\text{Pd}(^{19}\text{F},4n)$, at a beam energy of 74 MeV. The resultant γ rays were detected using standard γ -ray spectroscopic techniques with an array of six Compton-suppressed Ge detectors and a fourteen-element bismuth-germanate ball. The low-lying yrast structure is found to be dominated by the unique parity $\pi h_{11/2}$ orbital, manifest as a decoupled band with a large signature splitting. A crossing occurs in this band at $\hbar\omega_c = 0.42$ MeV, which is interpreted as $[\nu h_{11/2}]^2$ pair alignment. In addition, a strongly coupled negative-parity structure with large $B(M1)/B(E2)$ ratios is observed feeding both signatures of the $\pi h_{11/2}$ band. Bands built on the normal-parity $\pi g_{7/2}$ and $\pi g_{9/2}^-$ orbitals have also been confirmed and extended. These structures are compared to cranked-shell-model calculations and the systematics of the region.

I. INTRODUCTION

The neutron-deficient nuclei in the $A \approx 120$ –130 mass region have been of considerable interest in recent years. They lie in a transitional region between the primarily spherical (vibrational) tin ($Z=50$) nuclei, and the well-deformed lanthanum ($Z=57$) and cerium ($Z=58$) nuclei. The odd-iodine isotopes have recently been found to display a rich variety of nuclear structure: band termination has been found in $^{119,121}\text{I}$ [1], and single quasiparticle collective oblate and prolate structures have been observed to coexist in odd-mass $^{119-125}\text{I}$ [2]. This oblate stability has been attributed to the oblate-deformed $Z=54$ subshell gap [3]. In addition, the heavier Cs isotopes $^{127,131}\text{Cs}$ [4,5] have also shown near-oblate stability at higher rotational frequencies, due to the rotational alignment of a pair of upper-midshell $h_{11/2}$ neutrons.

These earlier measurements together with theoretical predictions [6,7] have led to the conclusion that the nuclei in this region are soft with respect to γ , the triaxiality parameter in the polar description of quadrupole shapes. In this mass region the proton Fermi surface lies in the lower part of the $h_{11/2}$ subshell, while the neutron Fermi surface lies in the $h_{11/2}$ midshell. Potential-energy-surface (PES) and cranked-shell-model (CSM) calculations suggest that these high- j valence particles exert a strong and specific driving force on the γ -soft core: Particles in the lower part of the $h_{11/2}$ subshell favor a collectively rotating prolate shape ($\gamma \approx 0^\circ$ in the Lund convention [8]), while those in the $h_{11/2}$ upper midshell favor a collectively rotating oblate shape ($\gamma \approx -60^\circ$).

The odd-mass Cs isotopes are expected to systematically display these characteristics, as the deformation remains well developed across a large range of the neutron Fermi surface. For these odd-proton nuclei, the signature splitting [9] of the band energies is sensitive to the configuration and the γ deformation. For the $\pi h_{11/2}$ band at lower rotational frequencies, the nucleus is close to prolate, producing a large signature splitting in the

yrast band. As the neutron Fermi surface increases across the isotopic chain, the magnitude of this signature splitting will change according to the position and softness of the energy minima of the configurations in β, γ space.

At higher rotational frequencies, pair alignment will occur, and the γ deformation may change depending on the nature of the aligning particles and the rigidity of the core. For ^{125}Cs the neutron Fermi surface is in a transitional region, where the favored γ value of the aligning pair is expected to vary substantially with the neutron number. The signature splitting of the neutron-aligned band is expected to decrease as the nuclear shape changes from prolate ($\gamma \approx 0$) through triaxial, and to vanish if the collective oblate ($\gamma \approx -60^\circ$) structure is achieved.

Low-lying states in ^{125}Cs have previously been determined following the β decay of ^{125}Ba by Arlt *et al.* [10], and coincident γ rays have been reported by Garg *et al.* [11] and Martin *et al.* [12]. The present paper reports experimental data on higher spin properties and additional band structures. The results are compared to CSM calculations and are discussed in terms of the systematics of the region. Odd-Cs results have previously been interpreted within the particle-rotor model [13].

II. EXPERIMENTAL METHODS AND RESULTS

Excited states in ^{125}Cs were populated with the fusion-evaporation reaction $^{110}\text{Pd}(^{19}\text{F},4n)$, at a beam energy of 74 MeV. The ^{19}F beam was provided by the Stony Brook FN tandem accelerator. The target consisted of 2.7 mg/cm² of ^{110}Pd rolled onto a lead backing of 50 mg/cm². The backing served to stop the recoiling nuclei, and thus minimize the Doppler shift in the γ -ray energies. The present series of experiments involved γ -ray excitation-function, γ - γ coincidence, and γ -ray angular distribution measurements.

A. Coincidence data

The γ -ray excitation functions and γ - γ coincidence data were obtained using an array of six n -type Ge detectors, each with an approximate efficiency of 25% relative to a 7.6 cm \times 7.6 cm NaI(Tl) detector for a γ -ray energy of $E_\gamma = 1332$ keV. The Ge detectors were located in a horizontal plane at angles of $+145^\circ$, $+78^\circ$, $+32^\circ$, -15° , -88° , and -145° with respect to the beam direction. Each Ge detector was operated in conjunction with a transverse bismuth germanate (BGO) shield [14], in order to reduce the Compton background. A coincidence resolving time of $2\tau = 100$ ns was used to collect the γ - γ data.

In addition, multiplicity information was collected with fourteen closely packed hexagonal BGO elements, seven above and seven below the target chamber. An energy threshold of 100 keV was set on each element, well above the Pb x rays. A hardware trigger requirement of at least two BGO elements and two Ge detectors was set in order to reduce the contribution to the data from Coulomb excitation and radioactivity. With this condition approximately 77×10^6 events were collected. These

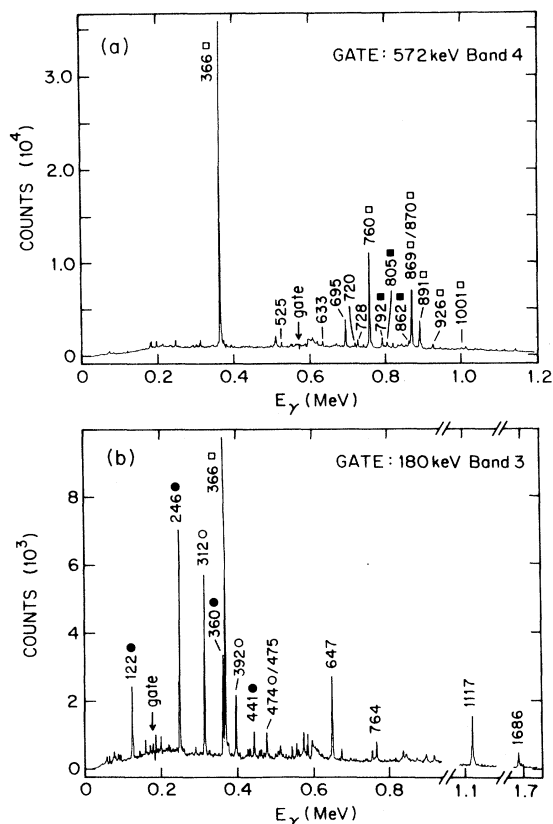


FIG. 1. Examples of gated coincidence spectra. The transition energies are labeled in keV. (a) A gate set on the 572 keV transition in band 4. Open (closed) squares indicate coincident transitions in the favored (unfavored) signature. (b) A gate set on the 180 keV transition in band 3. Open (closed) circles indicate coincident transitions depopulating the $\alpha = -\frac{1}{2}$ ($+\frac{1}{2}$) signature component.

data were subsequently sorted off-line to produce a symmetrized $2k \times 2k$ matrix, which was used in the construction of the level scheme of ^{125}Cs . Typical γ - γ coincidence spectra are shown in Fig. 1.

B. Angular distributions

The γ -ray angular distribution measurements were performed with two Compton-suppressed Ge detectors (CSG), each of similar specifications to those used in the coincidence experiments. One CSG, 22 cm from the target, was placed nonsequentially at angles of 90° , 115° , 125° , 135° , and 145° with respect to the beam direction. The second CSG, placed at -90° , served as a monitor. The empirical γ -ray intensities were fitted by the formula

$$W(\theta) = A_0 + A_2 P_2(\cos\theta) + A_4 P_4(\cos\theta),$$

where θ is the angle of the detector, P_n are Legendre polynomials, and A_n are adjustable parameters. The deduced A_2/A_0 and A_4/A_0 values for a number of $E2$ transitions were used to extract average empirical alignment parameters; $\alpha_2 = 0.85(10)$ and $\alpha_1 = 0.03(14)$ values were found to be consistent with all the bands in ^{125}Cs . Typical angular distributions for a $\Delta J = 2$ and two $\Delta J = 1$ transitions are shown in Fig. 2.

It was possible using these alignment parameters to extract $M1/E2$ mixing ratios for a number of $\Delta J = 1$ transitions by comparing experimental and theoretical [15] angular distribution coefficients within a χ^2 minimization technique [16]. The results of this analysis are included in Table I, which presents energies, relative intensities, angular distribution coefficients, mixing ratios, and spin and parity assignments for all the transitions assigned to ^{125}Cs (DCO ratios [17] provided no additional information, and are not included). The intensities are obtained from a combination of singles and coincidence data.

C. The decay scheme

The level scheme for ^{125}Cs deduced from the present series of measurements is shown in Fig. 3. The ordering

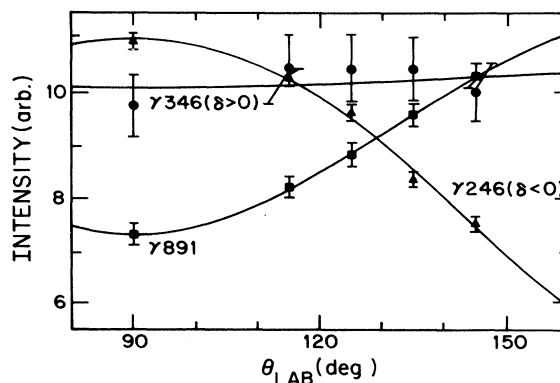


FIG. 2. Angular distributions for the $\Delta J = 1$, 246, and 346 keV and the $\Delta J = 2$, 891 keV transitions. The 246 keV dipole (band 3) is found to have a negative mixing ratio, while that for the 346 keV transition (band 2) is found to be positive.

TABLE I. Energies, relative intensities, angular distributions, and spin-parity assignments for the transitions assigned to ^{125}Cs following the $^{110}\text{Pd}(^{19}\text{F},4n)$ reaction at 74 MeV.

E_γ^a (keV)	Relative intensity ^b	A_2/A_0	A_4/A_0	Multipolarity Mixing ratio	$J_i^\pi \rightarrow J_f^\pi$
121.7	19(2)	-0.209(28)	-0.043(36)	$M1/E2$ $\delta = +0.30(6)$	$\frac{21}{2}^- \rightarrow \frac{19}{2}^-$
168.3	87(9)	+0.089(12)	-0.043(36)	$M1/E2$ $\delta = +0.22(2)$	$\frac{7}{2}^+ \rightarrow \frac{5}{2}^+$
176.0	64(6)	+0.115(13)	+0.019(16)	$M1/E2$ $\delta = +0.24(2)$	$\frac{7}{2}^+ \rightarrow (\frac{5}{2}^+)$
180.5	22(2)	-0.353(21)	-0.035(29)	$M1/E2$ $\delta = -0.66(30)$	$\frac{23}{2}^- \rightarrow \frac{21}{2}^-$
246.5	17(1)	-0.411(28)	-0.055(36)	$M1/E2$ $\delta = -0.34(19)$	$\frac{25}{2}^- \rightarrow \frac{23}{2}^-$
274.6	5(1)			$E1$	$\frac{9}{2}^+ \rightarrow \frac{11}{2}^-$
309.3	5(1)			$M1/E2$	$\frac{11}{2}^+ \rightarrow \frac{9}{2}^+$
311.8	20(1)	-0.395(24)	+0.020(31)	$M1/E2$ $\delta = -0.17(38)$	$\frac{27}{2}^- \rightarrow \frac{25}{2}^-$
346.5	4(1)	-0.020(72)	$\equiv 0$	$M1/E2$ $\delta = +0.14(1)$	$\frac{13}{2}^+ \rightarrow \frac{11}{2}^+$
359.5	8(1)	-0.545(39)	$\equiv 0$	$M1/E2$ $\delta = -0.19(3)$	$\frac{29}{2}^- \rightarrow \frac{27}{2}^-$
365.7	$\equiv 100$	+0.210(13)	+0.004(15)	$E2$	$\frac{15}{2}^- \rightarrow \frac{11}{2}^-$
378.1	6(1)			$M1/E2$	$\frac{15}{2}^+ \rightarrow \frac{13}{2}^+$
393.4	4(1)	-0.76(11)	+0.012(15)	$M1/E2$ $\delta = +0.39(14)$	$\frac{31}{2}^- \rightarrow \frac{29}{2}^-$
411.7	2(1)			$M1/E2$	$\frac{17}{2}^+ \rightarrow \frac{15}{2}^+$
430.2	7(1)	+0.518(60)	+0.073(74)	$E2$	$\frac{11}{2}^+ \rightarrow \frac{7}{2}^+$
438.9	2(1)			$M1/E2$	$\frac{19}{2}^+ \rightarrow \frac{17}{2}^+$
441.1	2(1)			$M1/E2$	$\frac{33}{2}^- \rightarrow \frac{31}{2}^-$
458.5(5)	<1			($E2$)	$\frac{17}{2}^- \rightarrow (\frac{13}{2}^-)$
470.2	≈ 1			$M1/E2$	$\frac{21}{2}^+ \rightarrow \frac{19}{2}^+$
474.3	<2			$M1/E2$	$\frac{35}{2}^- \rightarrow \frac{33}{2}^-$
474.7	9(2)	-0.609(43) ^c	-0.009(58) ^c	$M1/E2$ $\delta = -0.23(1)$	$\frac{19}{2}^- \rightarrow \frac{17}{2}^-$
489.2	<2			$M1/E2$	$\frac{23}{2}^+ \rightarrow \frac{21}{2}^+$
525.6	2(1)			($M1/E2$)	$(\frac{23}{2}^-) \rightarrow \frac{21}{2}^-$
554.3(5)	<1			($M1/E2$)	$(\frac{13}{2}^-) \rightarrow \frac{11}{2}^-$
558.4	<2			$E2$	$\frac{27}{2}^- \rightarrow \frac{23}{2}^-$
572.2	64(3)	+0.299(15)	+0.033(19)	$E2$	$\frac{19}{2}^- \rightarrow \frac{15}{2}^-$
583.9	<2			$E1$	$\frac{11}{2}^+ \rightarrow \frac{11}{2}^-$
607.0	<2			($E2$)	$(\frac{27}{2}^-) \rightarrow \frac{23}{2}^-$
610.3	7	+0.280(73)	-0.062(90)	$E2$	$\frac{15}{2}^+ \rightarrow \frac{11}{2}^+$
620	<2			($M1/E2$)	$(\frac{37}{2}^-) \rightarrow \frac{35}{2}^-$
620.5	5	+0.043(79) ^c	$\equiv 0^c$	$E2$	$\frac{21}{2}^- \rightarrow \frac{17}{2}^-$
634.3	<2			($M1/E2$)	$\frac{33}{2}^- \rightarrow \frac{31}{2}^-$
647.1	26	-0.700(23)	+0.061(31)	$M1/E2$ $\delta = -0.30(7)$	$\frac{17}{2}^- \rightarrow \frac{15}{2}^-$
655.8	2(1)	+0.67(16)	+0.12(20)	$E2$	$\frac{13}{2}^+ \rightarrow \frac{9}{2}^+$

TABLE I. (Continued).

E_γ^a (keV)	Relative intensity ^b	A_2/A_0	A_4/A_0	Multipolarity Mixing ratio	$J_i^\pi \rightarrow J_f^\pi$
670.2	<2			(E2)	$(\frac{23}{2}^-) \rightarrow \frac{19}{2}^-$
671.1	<2			E2	$\frac{29}{2}^- \rightarrow \frac{25}{2}^-$
686.0	<2			(E2)	$(\frac{31}{2}^-) \rightarrow (\frac{27}{2}^-)$
695.3	17	-0.640(27)	$\equiv 0$	M1/E2	$\frac{21}{2}^- \rightarrow \frac{19}{2}^-$
				$\delta = -0.25(1)$	
720.4	2(1)	-0.75(19)	$\equiv 0$	M1/E2	$\frac{29}{2}^- \rightarrow \frac{27}{2}^-$
				$\delta = -0.35(2)$	
725.0	≈ 1			E2	$\frac{15}{2}^+ \rightarrow \frac{11}{2}^+$
728.1	5(1)			M1/E2	$\frac{25}{2}^- \rightarrow \frac{23}{2}^-$
752.8	<2			E2	$\frac{31}{2}^- \rightarrow \frac{27}{2}^-$
759.5	35(3)	+0.346(21) ^c	+0.013(25) ^c	E2	$\frac{23}{2}^- \rightarrow \frac{19}{2}^-$
761.7	5(1)			(E2)	$\frac{19}{2}^+ \rightarrow \frac{15}{2}^+$
764.6	3(1)	-0.62(13)	+0.13(16)	M1/E2	$\frac{21}{2}^- \rightarrow \frac{19}{2}^-$
				$\delta = -0.25(15)$	
789.9	<2			E2	$\frac{17}{2}^+ \rightarrow \frac{13}{2}^+$
791.9	5(1)	+0.313(99)	+0.08(12)	E2	$\frac{25}{2}^- \rightarrow \frac{21}{2}^-$
797.5	<2			(E2)	$(\frac{31}{2}^-) \rightarrow (\frac{27}{2}^-)$
804.9	<2			(E2)	$\frac{33}{2}^- \rightarrow \frac{29}{2}^-$
819.4	<2			E2	$\frac{27}{2}^- \rightarrow \frac{23}{2}^-$
834.2	<2			E2	$\frac{33}{2}^- \rightarrow \frac{29}{2}^-$
850.7	<2			E2	$\frac{19}{2}^+ \rightarrow \frac{15}{2}^+$
854.5	<1			(E2)	$(\frac{37}{2}^-) \rightarrow \frac{33}{2}^-$
862.7	3(1)			E2	$\frac{29}{2}^- \rightarrow \frac{25}{2}^-$
864.3	2(1)			(E2)	$(\frac{23}{2}^+) \rightarrow \frac{19}{2}^+$
869				E2	$\frac{35}{2}^- \rightarrow \frac{31}{2}^-$
869.9	28(3)	+0.382(26) ^c	-0.014(32) ^c	E2	$\frac{27}{2}^- \rightarrow \frac{23}{2}^-$
888.6	<2			(E2)	$(\frac{23}{2}^+) \rightarrow \frac{19}{2}^+$
891.2	12(1)	+0.324(42)	-0.019(53)	E2	$\frac{31}{2}^- \rightarrow \frac{27}{2}^-$
909.2	<2			E2	$\frac{21}{2}^+ \rightarrow \frac{17}{2}^+$
915.5	<2			E2	$\frac{35}{2}^- \rightarrow \frac{31}{2}^-$
925.7	2(1)			(E2)	$(\frac{39}{2}^-) \rightarrow \frac{35}{2}^-$
944.2	<2			(E2)	$(\frac{35}{2}^-) \rightarrow (\frac{31}{2}^-)$
960.5	<2			E2	$\frac{23}{2}^+ \rightarrow \frac{19}{2}^+$
978.0	<2			(E2)	$(\frac{37}{2}^-) \rightarrow \frac{33}{2}^-$
1001.3	<2			(E2)	$(\frac{43}{2}^-) \rightarrow (\frac{39}{2}^-)$
1117.4	9(1)	-0.290(38)	$\equiv 0$	M1/E2	$\frac{19}{2}^- \rightarrow \frac{17}{2}^-$
				$\delta = -0.03(1)$	
1122.0	2(1)	+0.52(20)	$\equiv 0$	E2	$\frac{19}{2}^- \rightarrow \frac{15}{2}^-$
1143.0	≈ 1			(E2)	$(\frac{31}{2}^-) \rightarrow (\frac{27}{2}^-)$
1196.8	<2			(E2)	$(\frac{35}{2}^-) \rightarrow (\frac{31}{2}^-)$
1215.4	≈ 1			(E2)	$\frac{27}{2}^- \rightarrow \frac{23}{2}^-$
1221.0	<1			(E2)	$(\frac{23}{2}^-) \rightarrow \frac{19}{2}^-$
1315.5	<1			(E2)	$(\frac{27}{2}^-) \rightarrow \frac{23}{2}^-$
1366.6	2(1)	0.22(18)	$\equiv 0$	E2	$\frac{23}{2}^- \rightarrow \frac{19}{2}^-$

TABLE I. (Continued).

E_γ^a (keV)	Relative intensity ^b	A_2/A_0	A_4/A_0	Multipolarity Mixing ratio	$J_i^\pi \rightarrow J_f^\pi$
1686.4	4(2)	-0.13(10)	+0.03(13)	M1/E2 $\delta = +0.07(3)$	$(\frac{17}{2}^-) \rightarrow \frac{15}{2}^-$

^aGamma-ray energies are accurate to ± 0.3 keV, except those quoted as integers which are accurate to ± 1 keV, or as otherwise stated.

^bTransition intensities are corrected for Ge efficiency, and are obtained from a combination of singles and coincidence data.

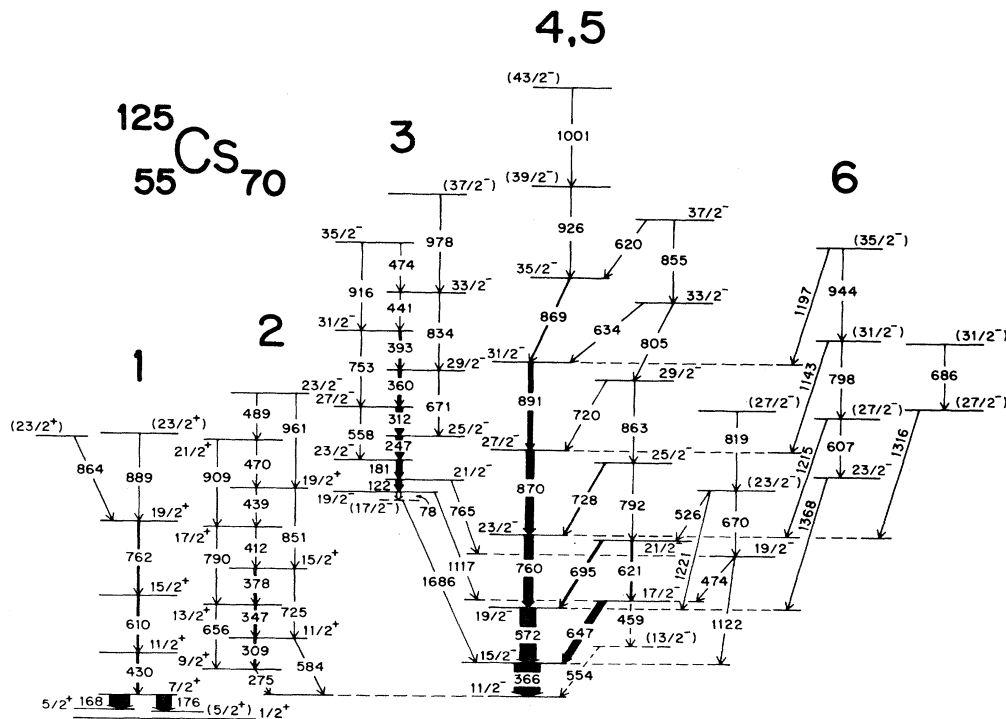
^cAngular distribution results quoted for the energy doublets 474.3/474.7, 620/620.5, 759.5, 761.7, and 869/869.9 keV which are unresolved in the singles data.

of the γ rays has been determined by coincidence relationships and relative intensities. Spins and parities have been assigned on the basis of angular distribution data and the systematics of the neighboring odd-Z nuclei. The levels naturally form several bands which have been labeled 1 to 6 in order to facilitate the discussion. The $\frac{1}{2}^+$ ground state and the 85 keV $\frac{5}{2}^+$ state have previously been identified by Arlt *et al.* [10] following the β decay of ^{125}Ba .

Bands 1, 2, and 4 have previously been observed by Garg *et al.* [11] up to spins of $\frac{19}{2}$, $\frac{15}{2}$, and $\frac{27}{2}$, respectively. To these bands they assign bandhead spins and parities of $\frac{7}{2}^+$, $\frac{9}{2}^+$, and $\frac{11}{2}^-$, respectively, based on angular distribution data, systematics of the region, and weak coin-

idence relations between states above and below the isomeric $\frac{11}{2}^-$ state. The results obtained from the present series of measurements are in good agreement with these assignments. In addition, Martin *et al.* [12] observed the favored signature of band 5 up to a spin of $\frac{43}{2}$. The present data are in agreement up to a spin of $\frac{39}{2}$, but indicate that the $\frac{43}{2} \rightarrow \frac{39}{2}$ transition has an energy of 1001 keV, in contrast to the previous assignment of 1080 keV.

Band 3 has been assigned a bandhead spin of $\frac{17}{2}$ based on the angular distributions observed for the three transitions decaying out of the band. The 1686.4, 1117.4, and 764.6 keV γ rays all have angular distributions consistent with $\Delta J=1$ multipolarities. Furthermore, band 3 has been assigned negative parity in accordance with the



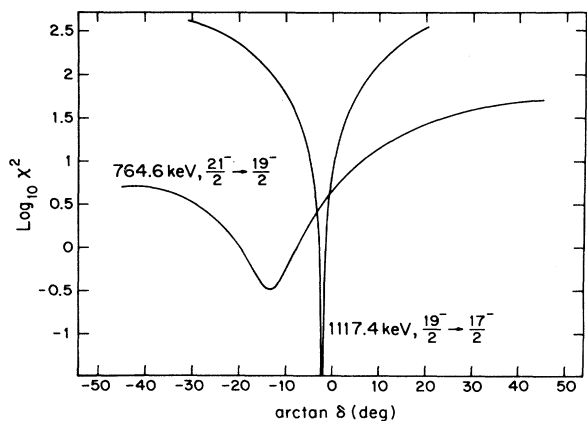


FIG. 4. $\log_{10}\chi^2$ versus $\arctan\delta$ for the 764 and 1117 keV transitions. Nonzero δ values are implied for both.

nonzero mixing ratios observed for the 764.6 and 1117.4 keV transitions, as is illustrated in Fig. 4.

III. DISCUSSION

In order to compare the experimental data with the CSM, the experimental spins and level energies have been transformed into the rotating frame of reference follow-

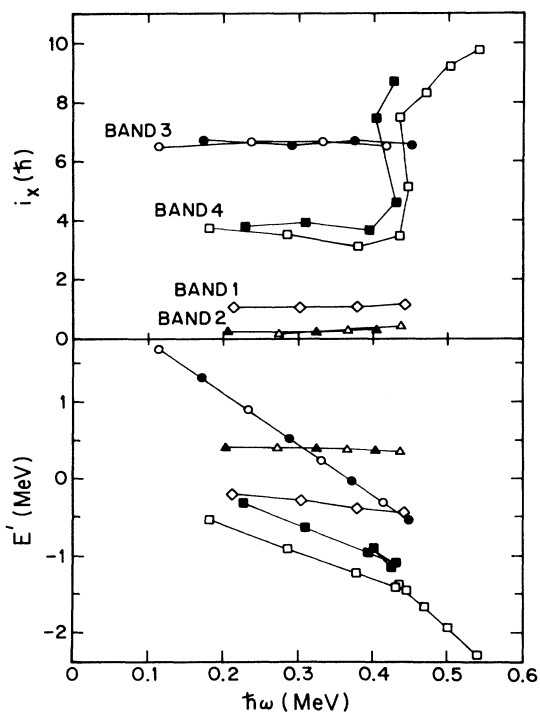


FIG. 5. Experimental Routhians and alignments for the positive-parity band 1 (diamonds) and band 2 (triangles), and the negative-parity band 3 (circles) and band 4 (squares). Filled (open) symbols are used for the signature component $\alpha = +\frac{1}{2}$ ($-\frac{1}{2}$).

ing the prescription of Bengtsson and Frauendorf [9]. The alignment i_x is defined as

$$i_x(\omega) = I_x(\omega) - I_{x,\text{ref}}(\omega),$$

where I_x is approximated by $I_x = [(J + \frac{1}{2})^2 - K^2]^{1/2}$, and $I_{x,\text{ref}}$ is a frequency-dependent reference characterized by a reference moment of inertia given by $\mathcal{J}_{\text{ref}} = \mathcal{J}_0 + \omega^2 \mathcal{J}_1$, with $\mathcal{J}_0 = 17.0 \hbar^2 \text{ MeV}^{-1}$ and $\mathcal{J}_1 = 25.8 \hbar^4 \text{ MeV}^{-3}$. The Harris parameters [18], \mathcal{J}_0 and \mathcal{J}_1 , have been obtained from a fit to the low-lying members of the $\pi h_{11/2}$ band in ^{123}Cs so that a systematic comparison of the alignments in the odd-mass Cs isotopes can be made. The experimental Routhians and alignments of the bands observed in ^{125}Cs are shown in Fig. 5. Quasiparticle configurations have been assigned to the bands in ^{125}Cs , and are summarized in Table II. These assignments will be discussed in the following sections.

A. Single-quasiparticle positive-parity bands

Band 1 is interpreted as being based on the positive parity quasiproton orbital originating from the $g_{7/2}[422]_{3/2}^+$ Nilsson state at a prolate deformation of $\beta_2 \approx 0.2$. The decoupled nature ($\Delta J = 2$) of this band is a consequence of the low- K value of $\frac{3}{2}$, with only the favored signature ($\alpha = -\frac{1}{2}$) being observed. The un-

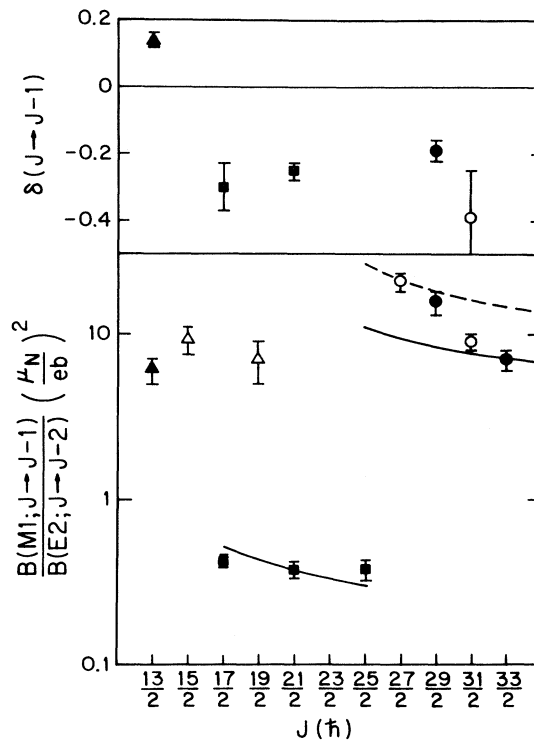


FIG. 6. Experimental $B(M1)/B(E2)$ ratios for a number of $\Delta J = 1$ transitions in band 2 (triangles), band 3 (circles), and band 4 (squares). Open (closed) symbols are used for transitions depopulating the signature component $\alpha = -\frac{1}{2}$ ($+\frac{1}{2}$). The corresponding $M1/E2$ mixing ratios are also displayed where available.

avored signature is expected to lie higher in energy. The angular distributions of the 430.2 and 610.3 keV transitions are consistent with their assigned stretched $E2$ nature (see Table I).

Band 2 is associated with a $g_{9/2}[404]_{\frac{9}{2}}^{+}$ proton-hole configuration which has systematically been observed in the Sb, I, and Cs isotopes [19, 20, 11]. The strongly coupled nature of this band is related to the large Ω value ($\Omega = \frac{9}{2}$) of the $\pi g_{9/2}$ orbital which originates from below the $Z=50$ spherical shell closure. The $\Delta J=1$ $M1/E2$ transitions linking the states of opposite signature are relatively strong compared to the crossover $E2$ transitions [$B(M1)/B(E2) \approx 10(\mu_N/e b)^2$; see Fig. 6], and exhibit zero signature splitting. It was possible to extract an $M1/E2$ mixing ratio $\delta = +0.14(1)$ for the 346.5 keV transition, which is consistent with the prolate deformation and the positive g factor of the $\pi g_{9/2}$ quasiparticle.

B. Single-quasiparticle negative-parity band

Band 4 has been assigned the unique-parity $\pi h_{11/2}[550]_{\frac{1}{2}}^{-}$ configuration. The band consists of two $\Delta J=2$ cascades, associated with the favored signature ($\alpha = -\frac{1}{2}$), based on the isomeric $\frac{1}{2}^{-}$ state, and the unfavored ($\alpha = +\frac{1}{2}$) signature. As expected for a low- K band, the signature splitting between the two cascades is large ($\Delta e' \approx 350$ keV, see Fig. 7). $\Delta J=1$ transitions are observed depopulating the unfavored signature to the favored: $B(M1)/B(E2)$ and mixing ratios have been extracted for lower spin transitions, and are displayed in Fig. 6. The geometrical model of Dönau and Frauendorf [21], however, underestimates these values by an order of magnitude when prolate axial symmetry and $K = \frac{1}{2}$ are assumed. This is consistent with previous experimental data in ^{131}La [22] and ^{127}Cs [4], where a similar enhancement of the $B(M1)/B(E2)$ ratio is observed. In Ref. [4] it was suggested that a degree of triaxiality would mix higher Ω components into the $\pi h_{11/2}$ band, producing a higher average K value, increasing the $B(M1)$ strength,

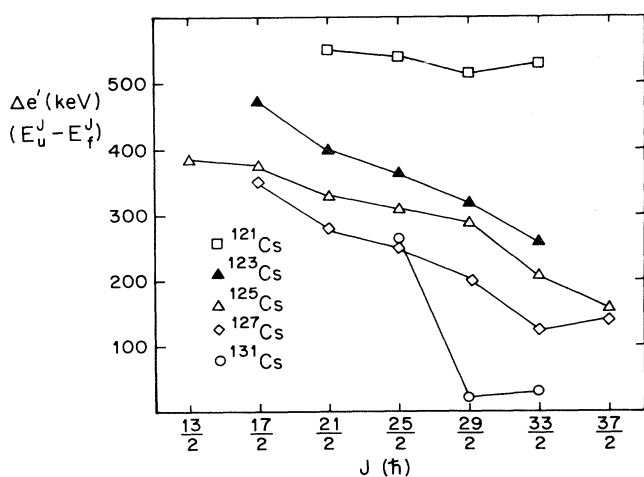


FIG. 7. The signature splitting $\Delta e'$ versus spin J for the yrast bands in a number of odd-mass Cs isotopes.

and additionally that it would reduce the $B(E2)$ strength [23]. In ^{125}Cs , values of $\gamma = 12^\circ$ and $K = \frac{3}{2}$ are consistent with the data. Total-Routhian-surface (TRS) calculations [24] predict that the favored signature of the $\pi h_{11/2}$ band is associated with a positive γ value ($\gamma \approx 10^\circ$), while the unfavored signature with a negative γ value ($\gamma \approx -10^\circ$). The effect on transition rates between states of different shapes is not well understood.

C. Band 6

Bands similar to band 6 have been observed systematically in this region in odd- Z ^{131}La [22] and ^{133}Pr [25] and even-even ^{126}Xe [30] and ^{128}Ba [33]. In the odd- Z nuclei these bands are characterized by strong $E2$ transitions depopulating each level to the favored signature of the yrast $\pi h_{11/2}$ sequence, with the intraband $E2$ transitions being relatively weak. In ^{125}Cs this structure is interpreted as a $\pi h_{11/2}$ quasiparticle coupled to the γ vibration of the core. The occurrence of this band at low excitation energies is further evidence of the γ softness in this nucleus. The structures of the sequences built on the $\frac{19}{2}^{-}$ and $\frac{27}{2}^{-}$ states are not clear, although they are most likely associated with the γ softness of the core.

D. Multiquasiparticle negative-parity bands

1. Band 5

Band 4, related to the $\pi h_{11/2}$ orbital, is crossed by band 5 at a rotational frequency of $\hbar\omega \approx 0.42$ (0.41) MeV in the favored (unfavored) signature, with a corresponding gain in alignment of $4\hbar$. This crossing is interpreted as being due to the rotational alignment of a pair of $h_{11/2}$ neutrons. The absence of any crossing below this frequency in other bands in ^{125}Cs suggests that the first proton crossing occurs at a higher frequency. This is in accordance with the systematics of the odd-mass Cs isotopes, where the neutron crossing has been observed in the yrast bands of $^{119-127,131}\text{Cs}$ [26, 5, 27, 4]. Figure 8 presents the alignments of these odd-mass Cs isotopes as a function of rotational frequency.

It is clear that the nature and strength of the interaction between the $\pi h_{11/2} \otimes [v h_{11/2}]^2$ band and the single $h_{11/2}$ proton band depends strongly on the position of the neutron Fermi surface. Figure 9 shows the results of

TABLE II. Quasiparticle configurations for the bands in ^{125}Cs .

Band	(π, α)	Configuration
1	$(+, -\frac{1}{2})$	$\pi g_{7/2}$
2	$(+, \pm\frac{1}{2})$	$\pi g_{9/2}^{-1}$
3	$(-, \pm\frac{1}{2})$	$v h_{11/2} \otimes v g_{7/2} \otimes \pi g_{7/2}$
4	$(-, \pm\frac{1}{2})$	$\pi h_{11/2}$
5	$(-, \pm\frac{1}{2})$	$\pi h_{11/2} \otimes [v h_{11/2}]^2$
6	$(-, -\frac{1}{2})$	$\pi h_{11/2} \otimes \gamma\text{-vib}$

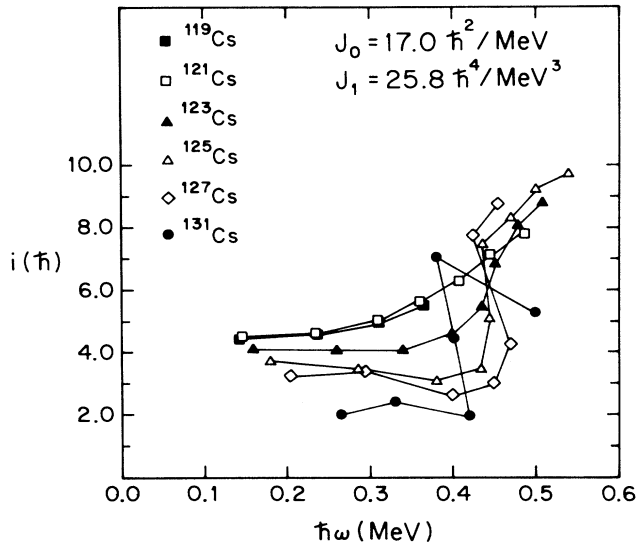


FIG. 8. The alignment i_x as a function of rotational frequency $\hbar\omega$ for the favored signature component of the yrast bands in a number of odd-mass Cs isotopes. A frequency dependent reference ($J_0=1.70\hbar^2 \text{ MeV}^{-1}$ and $J_1=25.8\hbar^4 \text{ MeV}^{-3}$) has been subtracted in each case.

a CSM calculation of the single quasineutron Routhian as a function of γ for a number of different locations of the neutron Fermi surface, ranging from $N=64$ (^{119}Cs) to $N=76$ (^{131}Cs). These results reveal the nature of the driving force of the neutron pair alignment on the core.

For the heaviest isotope ^{131}Cs , the aligning neutrons

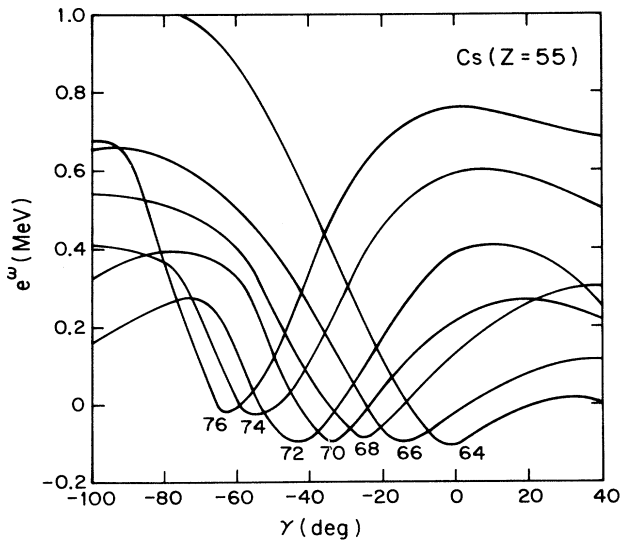


FIG. 9. Single quasineutron Routhians e' as a function of γ for a number of different locations of the neutron Fermi surface calculated within the CSM at a rotational frequency of $\hbar\omega=250$ keV. The calculation parameters Δ_N and ϵ_2 are obtained separately for each value of N from odd-even mass differences and TRS calculations, respectively. A value of $\epsilon_4=0$ is used.

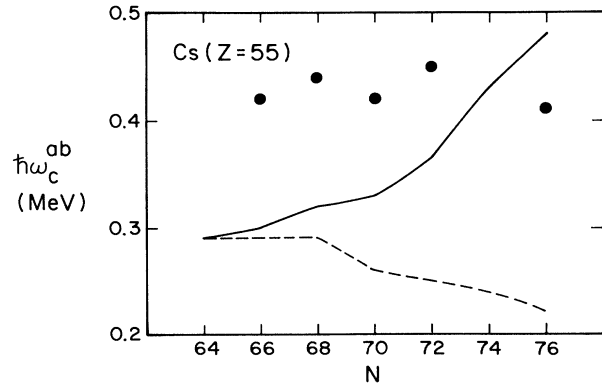


FIG. 10. The experimental crossing frequencies extracted from the yrast bands in a number of odd-mass Cs isotopes (circles), interpreted as the first neutron alignment. The solid line represents the CSM predictions assuming axial prolate symmetry, and the dashed line when a degree of triaxiality appropriate for the given isotope above the crossing is used.

strongly favor the collectively rotating oblate shape ($\gamma \approx -60^\circ$). The neutron polarizing effect is sufficient to induce a near-oblate shape, as is evident from the near-zero signature splitting of the aligned band. For the lighter isotopes $^{119,121}\text{Cs}$, however, the neutron Fermi surface is located such that a near-prolate shape with $\gamma \approx 0^\circ$ and $\approx -15^\circ$, respectively, is favored by the aligning neutrons. The signature splitting in the yrast bands of these nuclei remains large after the alignment, indicating that the nuclear shape remains close to prolate.

For the intermediate neutron Fermi surface in $^{123-127}\text{Cs}$, γ values in the range -25° to -45° are favored by the aligning neutrons. The signature splitting in the yrast bands of these nuclei shows a decrease as the spin increases, indicating a decrease in γ above the crossing. It is clear, however, that the collectively rotating oblate shape is not established in these nuclei.

In addition to the polarization effects, the location of the neutron Fermi surface will also be important in determining the strength of the interaction between the single and multi-quasiparticle bands. For neutron Fermi surfaces in the lower part of the $h_{11/2}$ subshell, the aligning neutrons will have a large wave-function spatial overlap with the $h_{11/2}$ proton, giving rise to a large interband interaction. This will be manifest as a smooth upbend in the alignment of the yrast band, over a large range of rotational frequencies, as is observed in $^{119,121}\text{Cs}$. Conversely, if the neutron Fermi surface is in the mid or upper $h_{11/2}$ subshell a smaller interband interaction will be expected, giving rise to a backbend in the alignment plots, as seen in $^{127,131}\text{Cs}$.

An additional insight into the nature of the crossing between the $\pi h_{11/2}$ and the $\pi h_{11/2} \otimes [v h_{11/2}]^2$ bands may be gained by examining the crossing frequency. The experimental crossing frequencies for the odd-mass Cs isotopes are displayed in Fig. 10. For the isotopes with a pronounced backbend, the crossing frequency is taken to be the frequency at which the experimental Routhians

cross in the usual manner, whereas for the isotopes with an upbend, the crossing frequency is estimated by extrapolating the alignments at low and high frequency to the crossing point. As can be seen from Fig. 10, the crossing frequencies remain remarkably constant across the isotopic chain. CSM calculation results are also displayed in Fig. 10. These results were obtained using the following parameter sets: the pairing gap parameters Δ_N were determined from neighboring odd-even mass differences, the quadrupole deformation parameters ϵ_2 were chosen to be consistent with TRS calculations, and $\epsilon_4=0$. It is clear that the CSM fails to reproduce the experimental data, both in the case where axial prolate symmetry is assumed and when a degree of triaxiality approximate for the aligned band in the given isotope is used.

For the lighter isotopes, the assumption of prolate axial symmetry is likely to be approximately valid both above and below the crossing. However, the large interaction between the crossing bands, not taken into account in the CSM, may be responsible for the large discrepancy observed between experiment and theory. For the heavier isotopes, where the band interaction strength is expected to be smaller, the effect of a large change in the γ value above and below the crossing will affect the crossing frequency. The CSM calculations are performed at a fixed β, γ deformation, and are therefore not likely to reproduce the data in a consistent manner.

2. Band 3

Negative-parity strongly coupled bands similar to band 3 have systematically been observed in even-even $^{120,124-128}\text{Xe}$ [28–31] and $^{124,126,128}\text{Ba}$ [12, 32, 33], and also in ^{127}Cs [4]. In the even-even nuclei, they have been assigned a $\nu g_{7/2} \otimes \nu h_{11/2}$ configuration, whereas in ^{127}Cs and for band 3 in ^{125}Cs , a configuration $\pi g_{7/2} \otimes \nu g_{7/2} \otimes \nu h_{11/2}$ is assigned. The strongly coupled nature arises from the $\Omega = \frac{7}{2} g_{7/2}$ neutron at a prolate deformation $\beta_2 = 0.2$. Band 3 is characterized by the $M1/E2 \Delta J = 1$ transitions, with negative mixing ratios

and large branching ratios [$B(M1)/B(E2) \approx 10(\mu_N/e b)^2$]. The g factor of the 8^- isomeric state in the corresponding band in ^{128}Xe has been measured [31] to be $-0.036(9)$. Using this value along with the empirical $\pi g_{7/2}$ g factor, and assuming $K = \frac{13}{2}$, it is possible to obtain good agreement with the experimental data using the Dönau and Frauendorf model. The large K value is consistent with those assigned to the corresponding bands in the Xe and Ba isotopes. The branching ratios also suggest that band 3 may contain a significant admixture of the pseudopartner $\pi d_{5/2}$, as they tend to be slightly larger than the predictions for the pure configuration assigned. In contrast to the alignment observed in the corresponding bands in the even-even Xe and Ba isotopes, band 3 has a large alignment of $i_x \approx 6\hbar$, which is due to the contribution of the low- Ω $\pi g_{7/2}$ orbital.

IV. CONCLUSIONS

Several rotational structures have been populated and observed in ^{125}Cs . Single quasiparticle bands based on proton $h_{11/2}, g_{7/2}$ and proton-hole $g_{9/2}$ orbitals, along with multiquasiparticle bands involving $h_{11/2}$ neutron alignment and $\pi g_{7/2} \otimes \nu g_{7/2} \otimes \nu h_{11/2}$ structures, are identified. The multiquasiparticle bands and band interaction characteristics are compared to the CSM and the systematics of the region.

The $\pi h_{11/2} \otimes [\nu h_{11/2}]^2$ band is found to be consistent with a triaxial shape, in accordance with the CSM. However, it is found that the CSM fails to reproduce the observed crossing frequency, as is the case for the other odd-mass Cs isotopes. The $\pi g_{7/2} \otimes \nu g_{7/2} \otimes \nu h_{11/2}$ structure is consistent with a prolate shape, and has $B(M1)/B(E2)$ ratios which are fully explained by the semiclassical model.

This work was supported in part by the National Science Foundation.

-
- [1] Y. Liang, D. B. Fossan, J. R. Hughes, D. R. LaFosse, R. Ma, T. Lauritsen, E. S. Paul, P. Vaska, M. P. Waring, N. Xu, and R. Wyss, *Phys. Rev. C* **44**, R578 (1991).
 - [2] Y. Liang, D. B. Fossan, J. R. Hughes, D. R. LaFosse, R. Ma, E. S. Paul, P. Vaska, N. Xu, and J.-y. Zhang, *Proceedings of the International Conference on High-Spin Physics and Gamma-Soft Nuclei*, Pittsburgh, 1990, edited by J. X. Saladin, R. A. Sorensen, and C. M. Vincent (World Scientific, Singapore, 1991), p. 104; M. P. Waring, D. B. Fossan, J. R. Hughes, D. R. LaFosse, Y. Liang, and P. Vaska, to be submitted to *Phys. Rev. C*.
 - [3] W. Nazarewicz, J. Dudek, R. Bengtsson, T. Bengtsson, and I. Ragnarsson, *Nucl. Phys.* **A435**, 397 (1985).
 - [4] Y. Liang, R. Ma, E. S. Paul, N. Xu, and D. B. Fossan, *Phys. Rev. C* **42**, 890 (1990).
 - [5] Y. Liang, Ph.D. thesis, Stony Brook, NY (1991).
 - [6] I. Ragnarsson, A. Sobczewski, R. K. Shelne, S. E. Larsson, and B. Nerlo-Pomorska, *Nucl. Phys.* **A233**, 329 (1974).
 - [7] Y. S. Chen, S. Frauendorf, and G. A. Leander, *Phys. Rev. C* **28**, 2437 (1983).
 - [8] G. Andersson, S. E. Larsson, G. Leander, P. Möller, S. G. Nilsson, I. Ragnarsson, S. Aberg, R. Bengtsson, J. Dudek, B. Nerlo-Pomorska, K. Pomorski, and Z. Szymański, *Nucl. Phys.* **A268**, 205 (1976).
 - [9] R. Bengtsson and S. Frauendorf, *Nucl. Phys.* **A327**, 139 (1979).
 - [10] P. Arlt, A. Jasinski, W. Neubert, and H.-G. Ortlev, *Acta Phys. Pol.* **B6**, 433 (1975).
 - [11] U. Garg, T. P. Sjoreen, and D. B. Fossan, *Phys. Rev. C* **19**, 217 (1979).
 - [12] J. P. Martin, V. Barci, H. El-Samman, A. Gizon, J. Gizon, W. Klamra, and B. M. Nyakó, *Nucl. Phys.* **A489**, 169 (1988).
 - [13] Ch. Droste, D. Chlebowska, J. Dobaczewski, F. Dönau, A. Kerek, G. Leander, J. Srebrny, and W. Waluś, *Nucl. Phys.* **A241**, 98 (1980).
 - [14] L. Hildingsson, C. W. Beausang, D. B. Fossan, W. F. Piel,

- Jr., A. P. Byrne, and G. D. Dracoulis, Nucl. Instrum. Methods **A252**, 91 (1986).
- [15] T. Yamazaki, Nucl. Data **A3**, 1 (1967).
- [16] R. D. Gill, *Gamma Ray Angular Correlations* (Academic, New York, 1975), p. 180.
- [17] K. S. Krane, R. M. Steffen, and R. M. Wheeler, Nucl. Data Tables **A11**, 351 (1973).
- [18] S. M. Harris, Phys. Rev. **138**, B509 (1965).
- [19] R. E. Shroy, A. K. Gaigalas, G. Schartz, and D. B. Fossan, Phys. Rev. C **19**, 1324 (1979).
- [20] W. F. Piel, Jr., P. Chowdhury, U. Garg, M. A. Quadar, P. M. Swertka, S. Vadja, and D. B. Fossan, Phys. Rev. C **341**, 456 (1985); R. E. Shroy, D. M. Gordon, M. Gai, D. B. Fossan, and A. K. Gaigalas, *ibid.* **26**, 1089 (1982).
- [21] F. Dönau and S. Frauendorf, in *Proceedings of the Conference on High Angular Momentum Properties of Nuclei, Oak Ridge, 1982*, edited by N. R. Johnson (Harwood Academic, New York, 1983), p. 143; F. Dönau, Nucl. Phys. **A471**, 469 (1987).
- [22] L. Hildingsson, C. W. Beausang, D. B. Fossan, R. Ma, E. S. Paul, W. F. Piel, Jr., and N. Xu, Phys. Rev. C **39**, 471 (1989).
- [23] A. L. Larabee, L. H. Courtney, S. Frauendorf, L. L. Riedinger, J. C. Wadington, M. P. Fewell, N. R. Johnson, I. Y. Lee, and F. K. McGowan, Phys. Rev. C **29**, 1934 (1984).
- [24] R. Wyss, Ph.D. thesis, Manne Siegbahn Institute, Stockholm (1990).
- [25] L. Hildingsson, C. W. Beausang, D. B. Fossan, and W. F. Piel, Jr., Phys. Rev. C **37**, 985 (1988).
- [26] P. Vaska, D. B. Fossan, J. R. Hughes, D. R. LaFosse, Y. Liang, and M. P. Waring, to be submitted to Phys. Rev. C.
- [27] J. R. Hughes, D. B. Fossan, D. R. LaFosse, Y. Liang, P. Vaska, and M. P. Waring, to be submitted to Phys. Rev. C.
- [28] K. Loewenich, K. O. Zell, A. Dewald, W. Gast, A. Gelberg, W. Lieberz, and P. Von Brentano, Nucl. Phys. **A460**, 361 (1986).
- [29] W. Gast, U. Kaup, H. Hanewinkel, R. Reinhart, K. Schiffer, K. P. Schmittgen, K. O. Zell, J. Wrzesinski, A. Gelberg, and P. Von Brentano, Z. Phys. **A318**, 123 (1984).
- [30] W. Lieberz, S. Freund, A. Grandrath, A. Gelberg, A. Dewald, R. Reinhart, R. Wirowski, K. O. Zell, and P. Von Brentano, Z. Phys. A **330**, 221 (1988).
- [31] T. Lönnroth, S. Vajda, O. C. Kistner, and M. H. Rafilovich, Z. Phys. A **317**, 215 (1984).
- [32] K. Schiffer, A. Dewald, A. Gelberg, R. Reinhart, K. O. Zell, Sun Xianfu, and P. Von Brentano, Z. Phys. A **327**, 251 (1987).
- [33] K. Schiffer, A. Dewald, A. Gelberg, R. Reinhart, K. O. Zell, Sun Xianfu, and P. Von Brentano, Nucl. Phys. **A458**, 337 (1986).